Optical properties of cosputtered gold-chromium alloy films*

W. Slusark, Jr.† and B. Lalevic

Department of Electrical Engineering, College of Engineering, Rutgers University, New Brunswick, New Jersey 08903

M. Ausloos

International Center for Theoretical Physics, ESIS, Université de Liège, Liege I, Belgium
(Received 7 November 1975; in final form 23 January 1976)

Optical properties of cosputtered thin-film (1500 Å) polycrystalline Au-Cr alloys have been investigated in the energy range 0.2–6.1 eV. Cosputtering of Au and Cr has extended the solubility limits of Cr in Au from 20 to 48 at.%. The reflectance data were analyzed by the Kramers-Kronig method and presented in terms of intraband and interband contributions. The observed frequency dependence of the relaxation time is explained on the basis of a two carrier mode. The shift in the Fermi level with increasing Cr concentration is found to be closer to the prediction of the Friedel theory than the rigid band model. The character of critical points for the interband transitions has been identified.

PACS numbers: 78.40.Kc, 73.60.Dt, 71.25.Pi

I. INTRODUCTION

The optical properties of the noble metals have been investigated in detail.[1] Comparison of theoretical band-structure calculations for the noble metals with experimental results has led to a general understanding of the electronic structure of these metals. It has been shown[2] that for the noble metals it is possible to unambiguously separate the intraband and interband components of the complex dielectric constant $\tilde{\epsilon}(\omega)$ using the classical Drude equations. Structure in the electronic absorption in the interband region has generally been attributed to transitions from the d band to the Fermi level, or from the Fermi level to the conduction level occurring at symmetry points in the Brillouin zone.

A considerable amount of theoretical and experimental work has been performed for gold.[1,3–11] Differences in sample preparation and experimental measurements have led to diverse results in the values of characteristic parameters and their frequency dependence. Reflectance measurements have been made on bulk electropolished samples,[3,7] thick evaporated layers,[1,4,5,8] and semitransparent films.[9,11] The electronic structure parameters have been shown to be dependent on the crystalline order and impurity content of the samples.[9] Relativistic band calculations for gold by Christensen and Seraphin[10] have correctly predicted the observed transition near 3.0 eV; however, they have not calculated the transition matrix elements. They have demonstrated that structure in the static reflection curves is not related to critical points in the band structure, whose contribution probably appears as fine structure only, which may or may not be near the broad peaks with which they must not be exclusively associated. The peaks must be associated with contributions from extended regions of $\vec{k}$ space.

The inclusion of transition-metal impurities in a noble-metal matrix yields useful information on the band structure of the noble metals. The important features of these alloys are movement of the noble-metal absorption edge on alloying, and the existence of new absorption peaks associated with virtual states of the impurity atom. Movement in the low-energy absorption spectrum of noble–transition-metal alloys is usually interpreted in terms of a rigid band model, or on a model developed by Friedel.[12] Optical absorption studies have been made on the following gold–transition-metal alloys: AuNi,[13] AuPd,[1,14] AuFe,[15] AuMn,[16] AuCr, and AuV.[17] The results reported for AuCr[17] alloys are for bulk mechanically polished samples up to a concentration of 20%Cr, i.e., the solubility limit of Cr in Au. The movement of the absorption edge on alloying was found to lie between the predictions of the rigid band model and Friedel's theory. Both parts of the main absorption edge were consistent with the assumption of d band to Fermi level transitions. Extra absorption bands associated with virtual states were reported in the region 1.2 eV from the Fermi level.

In this paper the optical properties of cosputtered thin-film (1500 Å) polycrystalline gold-chromium alloys in the energy range 0.2–6.1 eV have been investigated. In a previous paper,[18] the authors have shown that cosputtering of gold and chromium produces polycrystalline films in the entire compositional range up to the solubility limits of 49 at.% chromium in gold corresponding to the phase diagram of bulk material at 1100 °C. By cosputtering, a nonequilibrium high-temperature solubility of chromium in gold has been achieved at room temperature. This represents an extension of the concentration of chromium in gold previously investigated. We present in this paper the results and analysis of the optical properties of thin-film Au-Cr alloys in the extended solubility range. A detailed analysis of the optical behavior in the free-electron region is also given showing good agreement with recently proposed theoretical models.

II. EXPERIMENTAL

A. Sample preparation

Gold films and gold-chromium alloy films were rf cosputtered in a Norton Research Corporation triode sputtering system. Initial pressures were in the range 5×10^{-7} Torr. The background pressure of argon during sputtering was 1×10^{-3} Torr. Several thicknesses of each composition were made during a single run. Coat-

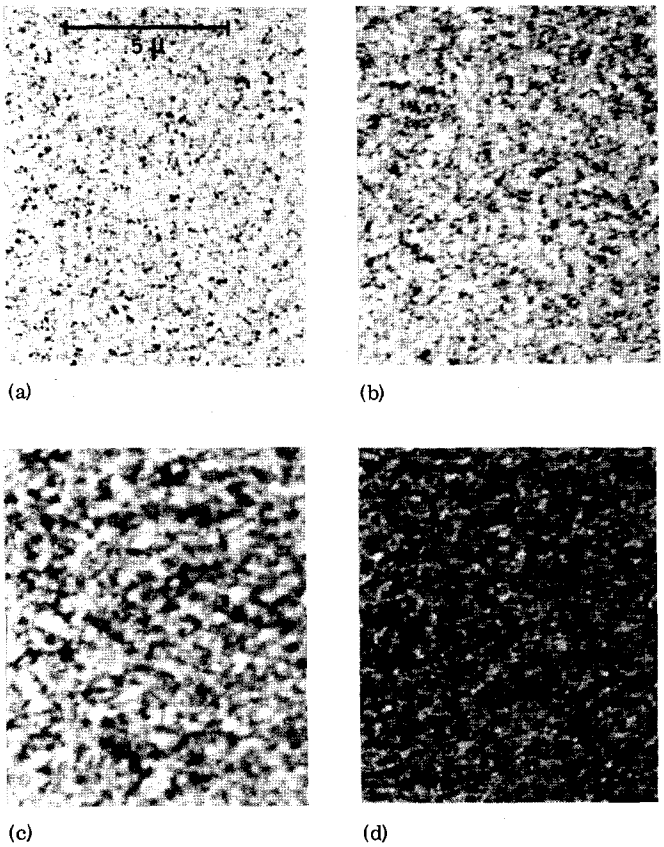

FIG. 1. Transmission micrographs of sputtered films: (a) 100-Å Au, (b) 200-Å Au, (c) 400-Å Au, (d) 400-Å Au (62 at.%)-Cr (38 at.%).

ings were simultaneously deposited on $\frac{1}{8}$-in. plate glass, which had been chemically cleaned, and SiO-coated electron microscope grids. Prior to sputtering, the substrates were subjected to electron glow discharge cleaning in 10×10^{-3} Torr of oxygen. Substrate temperatures during deposition of the films reached 150 °C. The sputtering rates decreased from 75 Å/min for pure gold to 25 Å/min for pure chromium.

Different compositions of gold-chromium were obtained by using a split-target configuration consisting of a gold foil partially overlapping an electroplated chromium target. By vertical displacement of the target mask, different ratios of gold and chromium were available for sputtering. The determination of the compositional range of the films was made by a preliminary measurement of the sputtering rate per unit area for the gold and chromium targets separately. Interference methods were used to obtain the thickness of selected thick films and thus determine a sputtering rate for that composition. With these values it was possible to obtain the contribution from each material in the composite target knowing their areas. The compositional range of the films was pure gold, 17 at.% chromium, 32 at.% chromium, 48 at.% chromium, and pure chromium.

The composition of the gold-chromium films was shown to be uniform by electron-probe microanalysis, in the limits of the resolution of that method. Further experimental detail can be found in our previous paper.[18]

Electron transmission and diffraction analysis showed polycrystalline films throughout the entire compositional range. The change in lattice constants of the cosputtered Au-Cr films, as determined from the diffraction patterns of the 400-Å films, showed exactly the same deviation from Vegard's law[18] as was found in bulk alloys at elevated temperatures.[19]

The transmission micrograph for a 100-Å gold film is shown in Fig. 1(a). As seen, the average crystallite size is approximately equal to the film thickness. Figures 1(b) and 1(c) show the transmission micrographs for 200- and 400-Å gold films. As the Au thickness is increased, the average crystallite size increases, but not proportionately. Figure 1(d) shows a transmission micrograph for a 400-Å 48-at.% chromium film. The average crystallite size is approximately 150—200 Å. In general, increasing chromium concentration resulted in decreasing crystal size for films of the same thickness. On this basis, we expect the average crystallite sizes in our 1500-Å films to be in the range 200—300 Å. This is confirmed by the high values of the resistivities obtained for these films and shown in Table I.

Toombs and Bennett[20] have studied the electrical resistivity of triode-sputtered gold films in the range 200—4000 Å. The films were deposited on glass substrates with varying substrate temperatures in the range 70—250 °C. They have found that the films exhibit a final resistivity about four times the value of bulk gold, which is in good agreement with the value reported in Table I for gold. They attribute this high value of resistivity to grain-boundary scattering due to small crystal size. They suggest that the smaller crystal size is a result of a high nucleation density due to the penetration of the substrate or film surface by high-energy sputtered gold atoms. The "tail" of their energy distribution forms new fixed nucleation sites which prevent the growth of large crystals. Cornely and Fuschillo[21] have reported initial nucleation densities of 1.2×10^{12} nucleated particles/cm^2 for gold films deposited under conditions similar to those of our films. They report an average crystal size of 85 Å for films greater than 100 Å thick.

Transmission and reflection measurements were made in air at room temperature in the range 0.2—2 μm using a Cary 14 double-beam double-monochromator ultraviolet—visible—near-infrared recording spectrophotometer. The reflectance attachment uses the W-V configuration of Strong.[22] The amplitude of the absorbance from sample to sample varied no more than 3% for films of equal thickness and composition. Reflectance measurements in the range 2—15 μm were made

TABLE I. Resistivity of Au-Cr films, 1500 Å thick, at 300 °K as a function of Cr concentration.

At.% Cr	100	48	32	17	Au (pure)
ρ (μΩ cm)	83.0	141.0	101.0	51.0	8.9

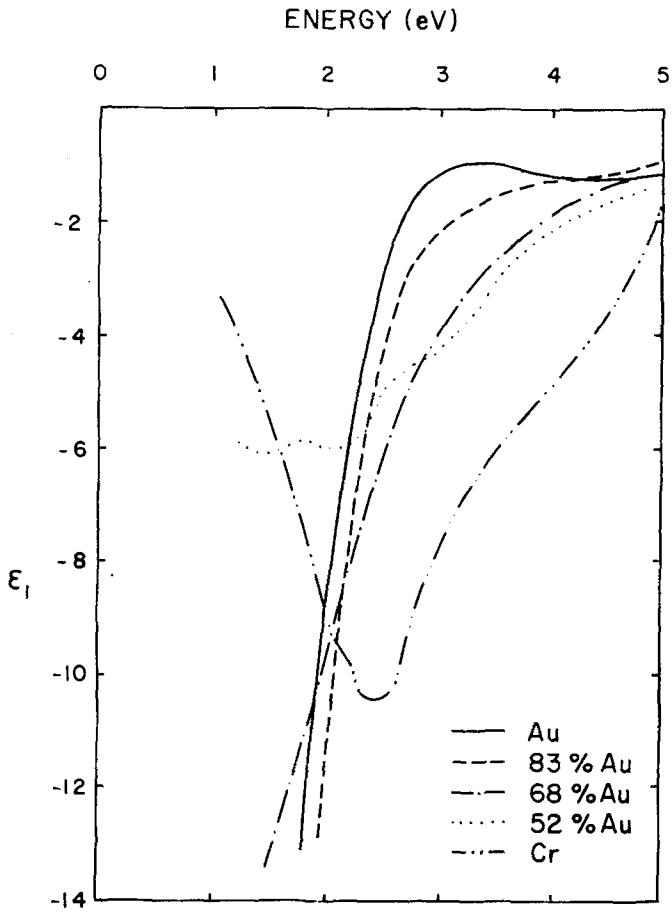

FIG. 2. ϵ_1 as a function of energy for Au, Cr, and Au-Cr alloys at $T = 300\,^{\circ}\mathrm{K}$.

on a Beckmann spectrophotometer for the 1500 Å films. The reflectance data as a function of composition for the 1500 Å films have been reported elsewhere.[23] The optical constants n and k, and ϵ_1 and ϵ_2 were calculated in the range 0.2—15 μm by a Kramers-Kronig analysis from the reflectance data of the 1500-Å films.

III. RESULTS AND DISCUSSION

Results of the application of the Kramers-Kronig analysis to the reflectance spectra of Au, Au-Cr, and Cr films are shown in Figs. 2 and 3. A plot of the real part of the dielectric constant ϵ_1 as a function of the incident radiation energy E is given in Fig. 2. The dependance of the imaginary part ϵ_2 on E is presented in Fig. 3, where the absorption coefficient ϵ_2/λ is plotted versus E. The analysis of the results presented in these figures in terms of the electronic structure of noble metals is customarily based[2,3] on a separation of free and bound electron contributions to the complex dielectric constant $\epsilon^* = \epsilon_1 + i\epsilon_2$. For free electrons (intraband transition) the complex dielectric constant is given by $\epsilon_f^* = \epsilon_1^f + i\epsilon_2^f$, and for bound electrons (interband transition) by $\epsilon_b^* = \epsilon_1^b + i\epsilon_2^b$.

A. Intraband transition

Experimental results for ϵ_1^f and ϵ_2^f can be analyzed in terms of the classical Drude theory or its later modifications. The real and imaginary parts of the dielectric constant are determined by the relaxation the τ and optical mass m_0 of conduction electrons in the following way:

$$\epsilon_1^f(\omega) = 1 - \frac{\omega_p^2}{\omega^2 + (1/\tau^2)}\,, \tag{1}$$

$$\epsilon_2^f(\omega) = \frac{\omega_p^2}{[\omega^2 + (1/\tau)^2]\omega\tau}\,, \tag{2}$$

where $\omega_p^2 = (2\pi c/\lambda_p)^2 = 4\pi N e^2/m_0$ is the plasma frequency and N is the density of conduction electrons.

Combining the above relations gives

$$\frac{\epsilon_2^f}{\lambda} = \frac{1}{2\pi c}\,\frac{\epsilon_1^f - 1}{\tau} \approx \frac{\epsilon_1^f}{2\pi c\tau}\,. \tag{3}$$

Therefore, a plot of ϵ_2/λ vs ϵ_1 yields the value for the relaxation time τ.

In the approximation $\omega \gg 1/\tau$, which is valid for noble metals at the near-ir region, the Drude relations can be written

$$\epsilon_1^f \approx 1 - \frac{\lambda^2}{\lambda_p^2}\,, \quad \epsilon_2^f = \frac{\lambda^3}{\lambda_p^2} = \frac{1}{\tau}\,. \tag{4}$$

Thus, ϵ_1^f depends on the optical mass m_0 only, and a plot of ϵ_1^f vs λ^2 gives the numerical value for m_0, N being known.

The plot of ϵ_2/λ vs ϵ_1 is given in Fig. 4 showing the frequency dependence of the relaxation time for Au, Au (83 at. %)-Cr (17 at. %), and Au (68 at. %)-Cr (32 at. %)

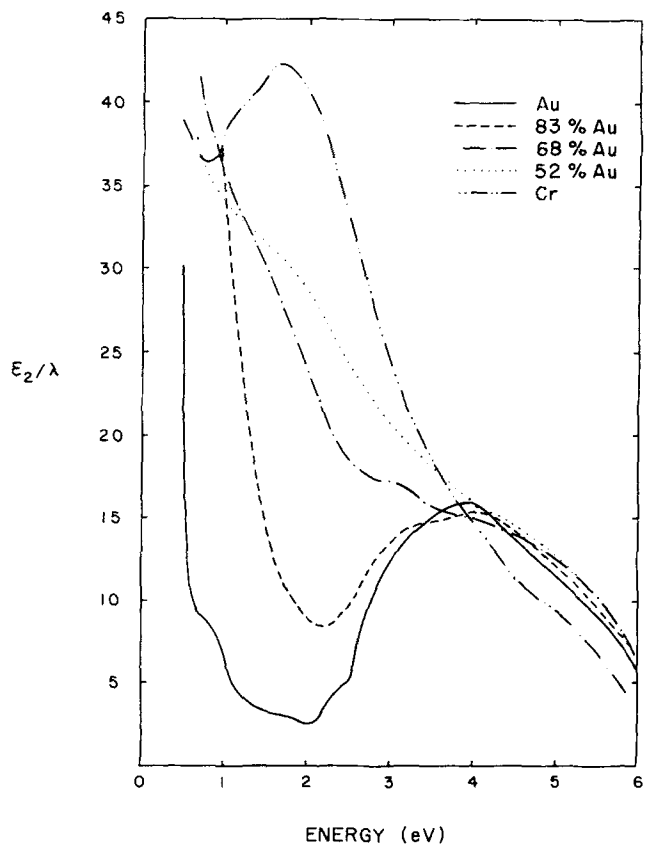

FIG. 3. Absorption coefficient ϵ_2/λ as a function of energy for Au, Cr, and Au-Cr alloys at $T = 300\,^{\circ}\mathrm{K}$.

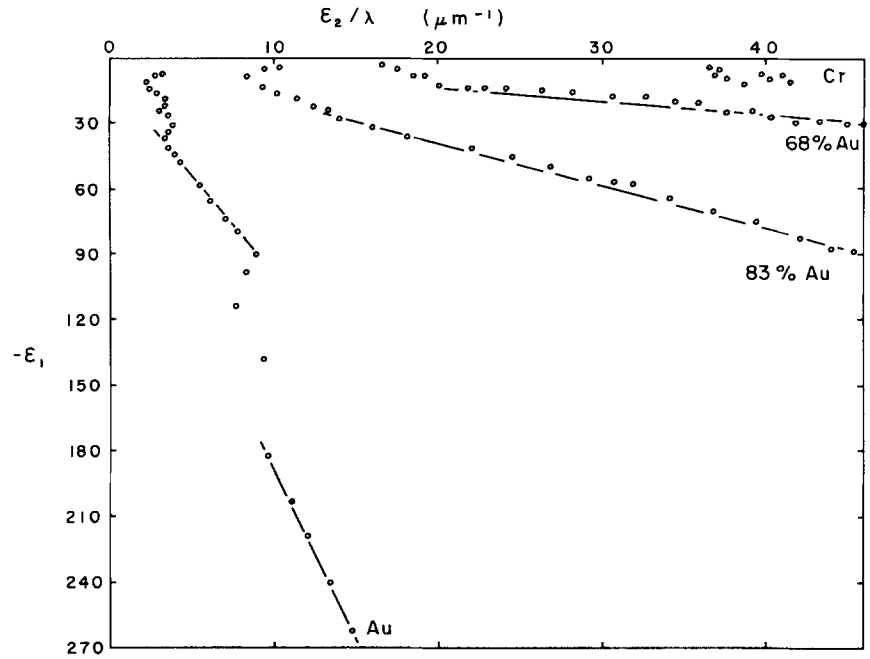

FIG. 4. Absorption coefficient ϵ_2/λ as a function of ϵ_1 for Au and Au-Cr alloys.

films. Pure Cr films had no region which obeyed the Drude relations. The values of the relaxation time as a function of energy and Cr concentration are listed in Table II, together with previously obtained data on pure Au films.

The frequency dependence of the relaxation time in Au has been obtained previously.[9,24] A way of interpreting the experimental results is to consider the Drude theory valid and define an effective relaxation time τ_{eff} in the form[25]

$$\left(\frac{1}{\tau}\right)_{\text{eff}} = -\frac{\omega\epsilon_2}{\epsilon_1 - 1} = a + b\omega^2, \quad \text{with a} = 1/\tau_0, \tag{5}$$

where τ_0 is the value of the optical relaxation time at zero frequency and b is a constant. Several theories have been advanced to explain a frequency-dependent term in $1/\tau_{\text{eff}}$. These theories are based either on the electron-electron interaction,[26] electron-phonon interaction,[25] or on the two-carrier model.[27] The first two theories do not include a dependence on the crystalline order; however, large variations of relaxation time with film structure have been observed.[9] In the two-carrier model,[27] electrons see a perfect lattice inside a crystallite and a disordered structure at areas between the crystallites. Therefore the electrons in these two regions could have different relaxation times. The frequency response of τ_{eff} in the two-carrier model is obtained by adding the responses of the two types of carriers, which results in the following expression:[27]

$$\left(\frac{1}{\tau}\right)_{\text{eff}} = \frac{1}{\tau_a}\left[1 + \frac{B}{A}\left(\frac{\omega^2 + \tau_a^{-2}}{\omega^2 + \tau_b^{-2}}\right)\right]^{-1} + \frac{1}{\tau_b}\left[1 + \frac{A}{B}\left(\frac{\omega^2 + \tau_b^{-2}}{\omega^2 + \tau_a^{-2}}\right)\right]^{-1}, \tag{6}$$

$$A = 4\pi N_a e^2/m_a, \quad B = 4\pi N_b e^2/m_b,$$

where N_a and N_b are the electron densities in the crystalline and disordered regions of a film and τ_a and τ_b are the relaxation times in the corresponding regions.

The plot of $(1/\tau)_{\text{eff}}$ vs $(\hbar\omega)^2$ for Au films is shown in Fig. 5. Using a computer curve-fitting procedure, the best agreement with Eq. (6) is obtained assuming $N_b/N_a = 0.15$ and $\tau_b/\tau_a = 0.025$. The plot of Eq. (6) using the

TABLE II. Relaxation time for Au and Au-Cr concentration for the energy of incident radiation E of 1.0 and 0.6 eV.

Composition	E	τ
Au	(in eV)	($\times 10^{-14}$ sec)
	1.0	0.51
	0.6	1.0
17 at.% Cr	1.0—0.6	0.14
32 at.% Cr	1.0—0.6	0.03 unannealed
Au (Ref. 9)	1.0	1.0 films
	0.6	2
	1.0	0.65
	0.6	0.76

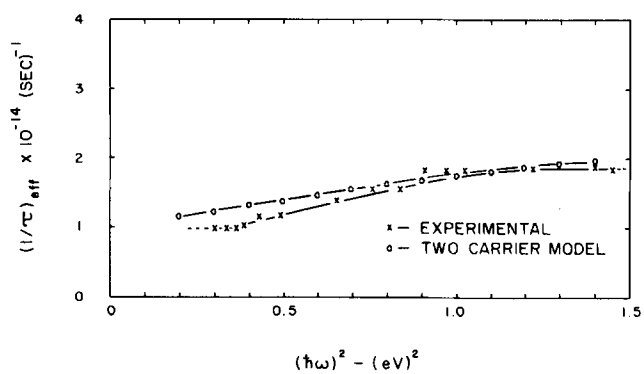

FIG. 5. Effective relaxation time as a function of the square of energy for Au. The theoretical curve is calculated from a two-carrier model.

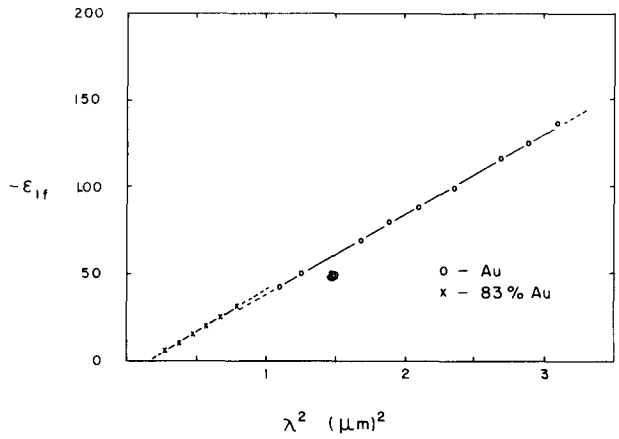

FIG. 6. Intraband contribution to ϵ_1 as a function of the square of the wavelength for Au and Au (83 at.%)-Cr (17 at.%).

above values for N_b/N_a and τ_b/τ_a is also given in Fig. 5, showing good agreement with the experimental results. Figure 5 also shows that the curves corresponding to both experimental data and the computer-fitted model are concave, indicating that Eq. (6) is a better fit of the data then a purely ω^2 dependence given by Eq. (5).

The plot of ϵ_1^f vs λ^2 for Au and Au (83 at.%)-Cr (17 at.%) films is given in Fig. 6. This plot gives the value for the optical mass according to Eq. (4). The optical mass for Au films thus found is $m_0 = 1.14$, assuming $N = 1$, which is in good agreement with previously published[8,11] values. The slope of ϵ_1 vs λ^2 for the Au (83 at.%)-Cr (17 at.%) film differs slightly from that in pure Au films in the region where $\omega > 1/\tau$ is applicable, as shown in Fig. 6. When corrections are made for the different atomic volumes of Au and Cr, a value of $m_0 = 1.39$ is obtained, assuming that Cr is divalent in Au. The optical mass for Au-Cr films with Cr concentration higher than 17% could not be determined due to a sharp decrease in the values of the relaxation time (Fig. 4) with increasing Cr concentration; thus there was no region where $\omega < 1/\tau$.

B. Interband transitions

Optical properties of the Au and Au-Cr alloy films

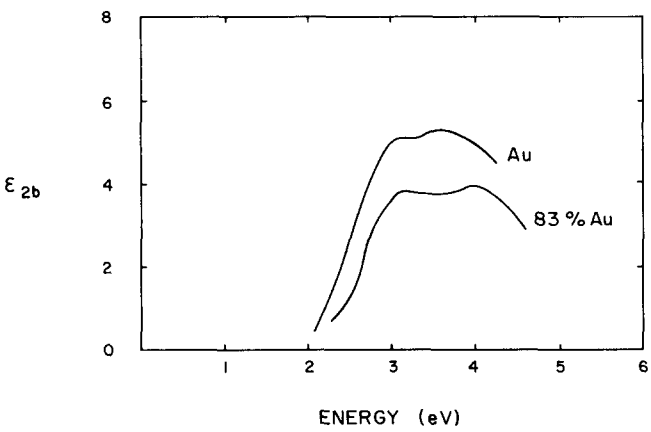

FIG. 7. Interband contribution to ϵ_2 as a function of energy for Au and Au (83 at.%)-Cr (17 at.%).

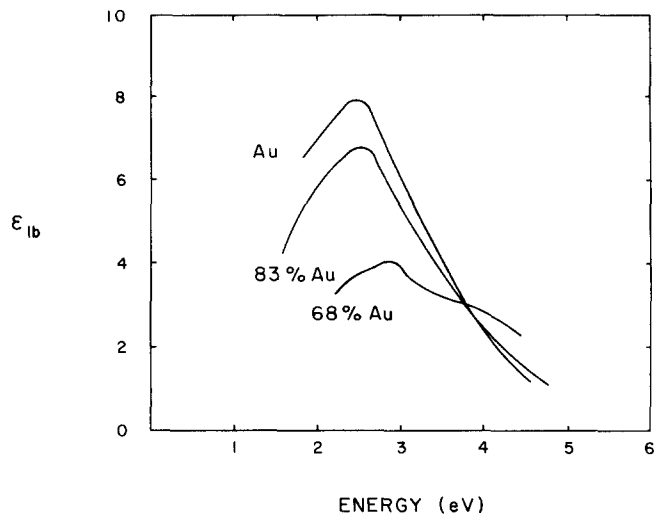

FIG. 8. Interband contribution to ϵ_1 as a function of energy for Au, Au (83 at.%)-Cr (17 at.%), and Au (68 at.%)-Cr (32 at.%).

due to interband transitions are determined by the absorptive part $\epsilon_2(\omega)$ of the dielectric constant, where the free-electron contribution $\epsilon_2^f(\omega)$ is subtracted from the experimental data. Figure 7 shows the plot of ϵ_2^b vs $\hbar\omega$ for Au and Au-Cr films. Associated with an absorption edge is also a peak[28] in $\epsilon_1^b(\omega)$. The plot of ϵ_1^b vs $\hbar\omega$ is given in Fig. 8. The shape of ϵ_2^b vs $\hbar\omega$ and the magnitude of maxima in ϵ_2^b for Au films are in agreement with recent measurements on evaporated Au films;[11] however, the magnitude is somewhat lower than observed in the earlier data on these films[8] and electropolished bulk specimen.[7] Identification of the peaks in ϵ_2^b and ϵ_1^b with the transition from the d band to the Fermi level and from the d band to the conduction band in pure Au films has been previously carried out.[2,7,9] The present data for Au films on $\epsilon_2^b(\omega)$ values as a function of frequency at 300 °K did not show any satellite peaks or new feature that has not been previously observed or discussed.

The shift in the maxima of $\epsilon_2^b(\omega)$ and $\epsilon_1^b(\omega)$ with alloying is associated with displacement of the absorption edge. The correct form of the absorption edge in Au has been calculated assuming a direct transition and constant matrix element.[10] The movement of the edge on alloying can be quantitatively predicted, assuming that the position of the edge represents the spacing between the top of the Au d bands and the Fermi surface. Thus, absorption edge displacement would correspond to the change in Fermi energy on alloying. This change can be calculated in the rigid band model approximation, which predicts a linear relationship with increasing Cr concentration, and Friedel's theory,[12] which takes into account screening effects and predicts a lower rate of change in the Fermi level on alloying.

The rigid band model assumes that the energy levels of the host material are unaffected by alloying. The only change is the increase (or decrease) of the Fermi level due to the different concentration of conduction electrons. The change in energy at the Fermi level upon alloying is given by[12]

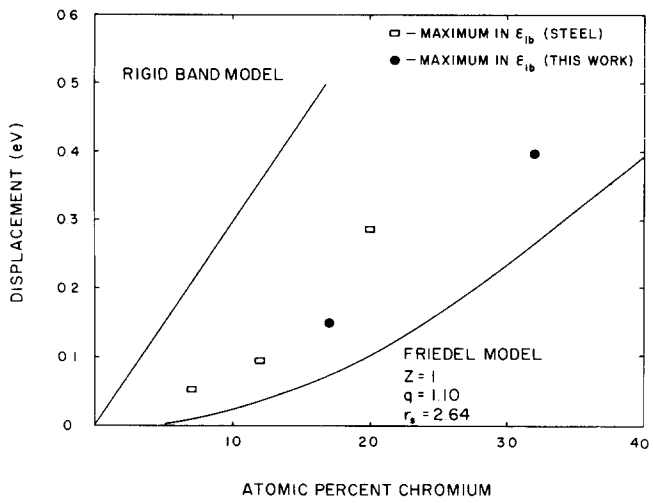

FIG. 9. Shift in Fermi level of Au-Cr alloys with chromium concentration. Previously obtained data on bulk Au-Cr alloys (Ref. 17) are also shown together with the predictions of the rigid band model and Friedel's model.

$$\Delta E = cZN/D(E_F), \tag{7}$$

where N is the atomic density of the impurity, c is the concentration of the impurity, Z the difference in valency between the host material and the impurity (here assumed to be one), and $D(E_F)$ is the density of states of the host material at the Fermi level (determined from low-temperature electronic specific-heat measurements). Using Friedel's model, the displacement of the Fermi level with alloying is given by

$$\Delta E = Zq/(qR\cosh qR - \sinh qR), \tag{8}$$

where

$$(qR)^{-3} = (qr_s)^{-3}c \tag{9}$$

and R is the screening radius, r_s is the radius of the atomic sphere of the impurity (2.64 Å for chromium), and q is the screening parameter (1.1) determined from the density of states function.

The shift in the first peak in $\epsilon_2^b(\omega)$ and $\epsilon_1^b(\omega)$ with increasing Cr concentration is shown in Fig. 9. Previously obtained data on bulk Au-Cr alloys[17] in the limits of the equilibrium solid solubility are also shown in Fig. 9, together with the rigid band and Friedel's model predictions. As seen from Fig. 9, the experimental data on the edge movement with increasing Cr concentration lie closer to Friedel's curve, especially at higher concentrations. The calculated curves are based on the assumption that Cr is divalent when dissolved in Au. Unfortunately this cannot be checked exactly, since the ir data gives only the ratio n_{eff}/m_0, where n_{eff} is the effective number of free carriers. However, the combination of the sum rule and the data of the optical mass obtained from Fig. 6 indicates that the above assumption is correct. In general, only a very large change in Cr valency would bring the theoretical curve (Fig. 9) in agreement with experiments.

The change on alloying in the effective number of electrons contributing to the optical properties up to a given frequency ω_0 can be estimated from the sum rule

$$\int_0^{\omega_0} \omega\epsilon_2(\omega)\,d\omega = \frac{2\pi^2 Ne^2}{m}\,\frac{n_{eff}}{m_0}, \tag{10}$$

where N is the atomic density. A plot of n_{eff} vs $\hbar\omega_0$ is obtained by numerical integration of the experimental values for $\epsilon_2(\omega)$ and is given in Fig. 10(a). In the free-electron region at low energies, for the Au films, $n_{eff} = 1$ electron/atom at the mass $m_0 = 1.14$. The rise in n_{eff} at 2 eV is due to the onset of interband transitions. For Au (83 at.%)-Cr (17 at.%) films, n_{eff} saturates at the value of 1.23 electron/atom. Assuming the optical mass m_0 increases as determined from Fig. 6, the number of electrons per atom would correspond to an assigned value of at least 2 for Cr in Au-Cr alloys.

The sum rule for the energy loss function $-I_m\epsilon^{-1}(\omega)$ given by

$$-\int_0^{\omega_0} \omega I_m\epsilon^{-1}(\omega)\,d\omega = \frac{2\pi^2 Ne^2}{m}\,\frac{n_{eff}}{m_0} \tag{11}$$

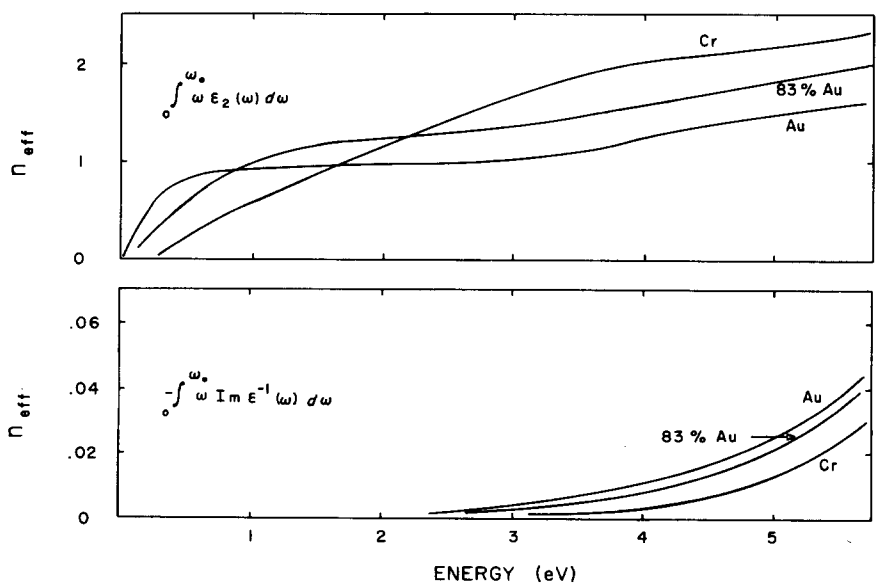

FIG. 10. Effective number of electrons as a function of energy for Au, Cr, and Au-Cr alloys as obtained from the sum rules.

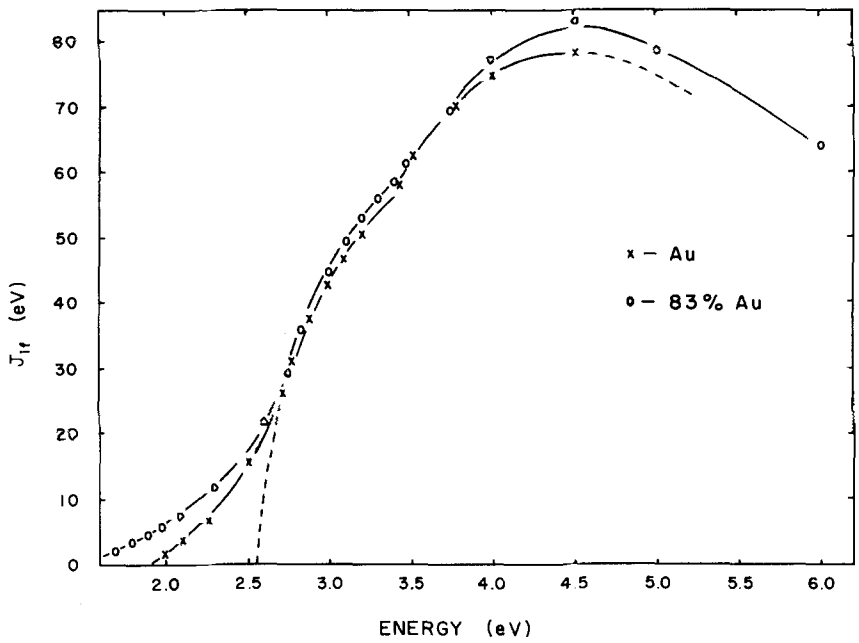

FIG. 11. Joint density of states as a function of energy for Au and Au (83 at.%)-Cr (17 at.%).

is indicative of the large losses at plasma resonance. The plot of n_{eff} corresponding to the $-I_m\epsilon^{-1}(\omega)$ sum rule is given in Fig. 10(b). The plots are quite smooth, indicating the absence of plasma affects in Au and Au-Cr films.

Information about the joint density of states J_{if} and the nature of critical points can be obtained from the $\epsilon_2^b(\omega)$ dependence on frequency. The joint density of states J_{if} is given by[29]

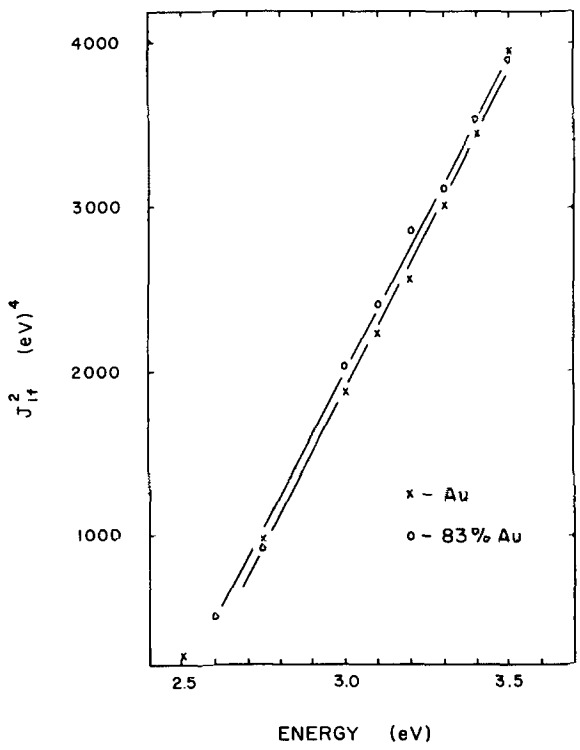

FIG. 12. Parabolic dependence of the joint density of states as a function of energy in the region 2.5—3.5 eV.

$$J_{if}=\frac{1}{8\pi^3}\int\frac{dS}{|\nabla_k E_{if}|}=\frac{1}{8\pi^3}\int\delta(E_{if}(k)-\hbar\omega)\,dk \quad (12)$$

and is related to $\epsilon_2^b(\omega)$ by

$$J_{if}(\omega)=(\hbar\omega)^2\epsilon_2^b(\omega). \quad (13)$$

The plot of J_{if} vs $\hbar\omega$ for Au and Au (83 at.%)-Cr (17 at.%) films is presented in Fig. 11, showing three distinct regions in the $J_{if}(\omega)$ dependence of energy.

In the region from 2.5 to 3.5 eV, the functional relationship between $J_{if}(\omega)$ and energy is parabolic. The parabolic dependence is shown in Fig. 12, where $J_{if}^2(\omega)$ is plotted against $\hbar\omega$. This represents a well-known square-root relation between $J_{if}(\omega)$ and energy as given by [29]

$$J_{if}(\omega)=\frac{[E(k)-E(k_0)]^{1/2}}{4\pi^2(\beta_1\beta_2\beta_3)^{1/2}}=a(\hbar\omega-\hbar\omega_0)^{1/2}, \quad (14)$$

where β_1, β_2, and β_3 are coefficients in the relation $E=E(k^2)$. The relation (14) represents M_0-type critical points. The onset energy $\hbar\omega_0$ can be determined accurately from Fig. 12, and the values obtained are $\hbar\omega_0=2.56$ eV for Au film and $\hbar\omega_0=2.58$ eV for Au (83 at.%)-Cr (17 at.%) film. Thus, there is a shift in the onset energy with the addition of Cr to Au. This shift is approximately equal to the shift in the $\epsilon_2^b(\omega)$ maximum with increasing Cr concentration (Fig. 9).

The region from 3.5 to 4.5 eV also exhibits parabolic behavior of J_{if} and a maximum in J_{if} at 4.5 eV. A similar behavior was observed previously in Au[9] and Cr.[30] It was suggested[30] in this case that the observed $J_{if}(\omega)$-vs-$\hbar\omega$ shape is typical of transition at an M_2 saddle-type critical point of the joint density of states, where

$$J_{if}(E)\approx C\{1-[E(k)-E(k_0)]^{1/2}\}. \quad (15)$$

From consideration of the M_2 critical point, it was further suggested that the second maximum in $\epsilon_2^b(\omega)$ corresponds to the transition from the conduction band below the Fermi level to the upper conduction band at

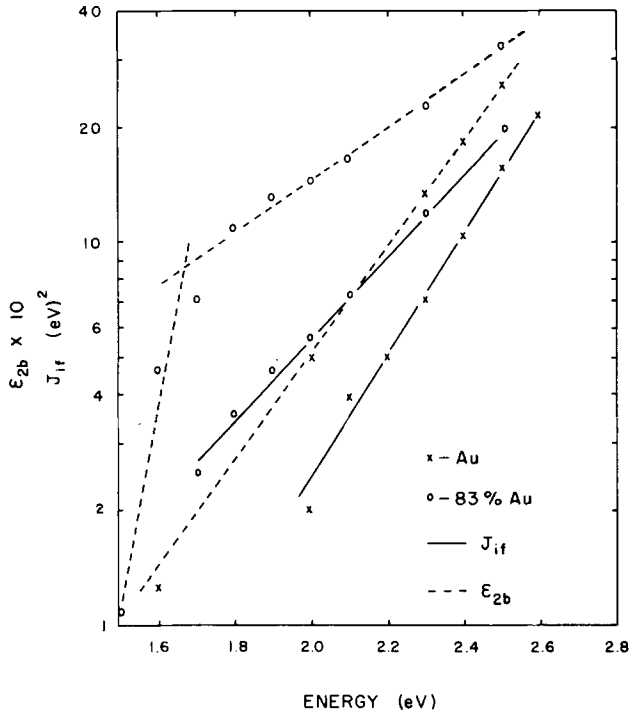

FIG. 13. Exponential dependence of joint density of states and interband contribution to ϵ_2 as a function of energy in the region 1.7–2.5 eV.

L. As seen from Fig. 11, the maximum in $J_{if}(\omega)$ at 4.5 eV is larger in Au-Cr films than in Au films.

In the region between 1.7 and 2.5 eV, i.e., below the onset of interband transitions, an exponential dependence of $J_{if}(\omega)$ and $\epsilon_2^b(\omega)$ on $\hbar\omega$ is observed, as shown in Fig. 13. The numerical values of $J_{if}(\omega)$ and $\epsilon_2^b(\omega)$ for Au films are in agreement with previously reported data.[9] The addition of Cr and Au changes both the magnitude and slopes of $J_{if}(\omega)$ and $\epsilon_2^b(\omega)$ in this energy region. An additional structure below 1.7 eV can be seen in Au-Cr films. The absorption tail in the 1.7–2.5-eV region was found to be insensitive to the film structure,[9] indicating that it is not due to defects. It is assumed that the absorption tail is an intrinsic property related to the direct interband transition. The additional structure in $J_{if}(\omega)$ and $\epsilon_2^b(\omega)$ of Au-Cr films can be related to the stress induced on alloying, since the observed structure is very similar to one previously observed in piezoreflectance measurements.[31]

IV. CONCLUSIONS

An analysis of the optical properties of the Au-Cr alloy films has shown the relaxation time in the intraband region to be frequency dependent. Comparison with different theories treating the frequency dependence has shown that the effect can be best explained in terms of a two-carrier model.

The movement of the absorption edge in Au with increasing concentration of Cr was studied in the interband region. It was found that the shift in the Fermi level with increasing Cr concentration lies closer to the predictions of the Friedel theory than that of the rigid band model approximation, assuming divalency of Cr in Au. The sum rule and the ϵ_1^f-vs-λ^2 plot indicate that Cr is at least divalent when dissolved in Au. The critical point for the absorption edge at 2.5 eV is of the M_0 type, while in the interband transition above 3.5 eV, it is a saddle-type M_2 critical point.

*Work supported by the Pittsburgh Plate Glass Industry.
†Holder of NSF traineeship.
[1]F. Abeles, *Optical Properties and Electronic Structure of Metals and Alloys*, edited by F. Abeles (North-Holland, Amsterdam, 1966).
[2]H. Ehrenreich and H.R. Phillipp, Phys. Rev. 128, 1622 (1962).
[3]B.R. Cooper and H. Ehrenreich, Phys. Rev. 138, A494 (1965).
[4]L.G. Schulz, J. Opt. Soc. Am. 44, 540 (1954).
[5]J.E. Davey and T. Pankey, J. Appl. Phys. 36, 2571 (1965).
[6]R.A. Ballinger and C.A. Marshall, J. Phys. C. 2, 1822 (1969).
[7]G.P. Pells and M. Shiga, J. Phys. C. 2, 1835 (1969).
[8]J. Hodgson, J. Phys. Chem. Solids 29, 2175 (1968).
[9]M.L. Théye, Phys. Rev. B 2, 3060 (1970).
[10]N.E. Christensen and B.O. Seraphin, Phys. Rev. B 4, 3321 (1971).
[11]P.B. Johnson and R.W. Christy, Phys. Rev. B 6, 4370 (1972).
[12]J. Friedel, Adv. Phys. 3, 446 (1954).
[13]F. Abeles, *Metallic Solid Solutions*, edited by J. Friedel and A. Guinier (W.A. Benjamin, Inc., New York, 1963).
[14]H.P. Meyers, L. Walden, and A. Karlsson, Philos. Mag. 18, 725 (1968).
[15]D. Beaglehole and T.J. Hendrickson, Phys. Rev. Lett. 22, 133 (1969).
[16]M.R. Steel and D.M. Treherne, J. Phys. F 2, 199 (1972).
[17]M.R. Steel, J. Phys. F 2, 605 (1972).
[18]W. Slusark, Jr., B. Lalevic, and N. Fuschillo, J. Appl. Phys. 44, 2891 (1973).
[19]E. Raub, Z. Metallkd. 51, 290 (1960).
[20]P. Toombs and P. Bennett, J. Appl. Phys. 39, 2984 (1968).
[21]R.H. Cornely and N. Fuschillo, J. Vac. Sci. Technol. 11, 163 (1974).
[22]J. Strong, *Procedures in Experimental Physics* (Prentice-Hall, New York, 1938).
[23]N. Fuschillo, B. Lalevic, W. Slusark, Jr., and A. Delahoy, J. Vac. Sci. Technol. 12, 84 (1975).
[24]H.E. Bennett, T.M. Bennett, E.T. Ashley, and R.J. Motyka, Phys. Rev. 165, 755 (1968).
[25]T.T. Hoffield, AIP Conf. Proc. 4, 358 (1972).
[26]R.N. Gurzhi, M.Y. Azbel, and H.P. Lin, Sov. Phys.-Solid State 5, 554 (1963).
[27]S.R. Nagel and S.E. Schnatterly, Phys. Rev. B 9, 1299 (1974).
[28]B. Velicky, Czech. J. Phys. B11, 787 (1961).
[29]F. Wooten, *Optical Properties of Solids* (Academic, New York, 1972).
[30]U. Gerhardt, Phys. Rev. 172, 651 (1968).
[31]M. Garfinvel, T.T. Tiemann, and W.E. Eugler, Phys. Rev. 148, 695 (1966).